IBN SINA

Ibn Sina Journal of Medical Science, Health & Pharmacy
Vol. 2, No. 1, 2025, pp. 1-8
ISSN 3104-6428
https://ibn-sina-journal-of-medical-sciences.jo

Zn-Ni-Co Ternary Oxide/Carbon nanotubes Nanocomposites Electrode Material for high performance Energy Storage in Medical Applications

Laith Alzboon [a,1,*], Saddam Almajali[b,2]

[a] Phd, Department of Nursing, university of Jordan, Jordan, Irbid, Email:
[b] Phd, Department of Nursing, university of Jordan, Jordan, Irbid, Email:

* Corresponding Author

ARTICLE INFO

Article history
Received May 15, 2025
Revised May 19, 2025
Accepted June 22, 2025

Keywords
Supercapacitors;
cycling stability;
carbon nanotubes;
Zn−Ni−Co ternary oxide (ZNC),
energy storage.

ABSTRACT

INTRODUCTION: The growing demand for portable power sources such as electric vehicles and hybrid electric vehicles has inspired much interest in developing advanced energy storage devices for practical applications. Among these energy storage systems, supercapacitors have attracted extensive attention because of their higher power density and cycling stability than batteries, as well as their higher energy density than conventional electrolytic capacitors.

METHODS: Among the metal oxides, Zn−Ni−Co ternary oxide (ZNC) has attracted particular interest recently because of its superior electrochemical properties. In the present work, we explored porous ZNC / carbon nanotubes (CNTs) (ZNC/CNTs) in the form of hexagonal nameplates.

RESULTS: This material has got various advantages, such as high surface area, effective electrolyte/electrode interaction, superior electron/ion transportation, and promising strain accommodation. Moreover, the electrochemical characterizations showed that the as-synthesized composite electrode demonstrated a synergistic effect between the CNTs and the porous ZNC, resulting in favourable pseudocapacitive behaviour, including good specific capacitance, high rate performance, and excellent cycling stability. These advantages, along with the simple processing technique, make this ZNC-CNTs composite a potential candidate for pseudocapacitive applications. In particular, this

CONCLUSION: CNT wrapped multi-cationic metal oxide with a homogeneous structure exhibited a high specific capacitance of 2360 F g−1 at a current density of 2 A g-1 with remarkable cycling stability, 96% capacitance retention after 10000 cycles of charge-discharge. The CNTs wrapped around the ZNC ensure a short ion diffusion distance, percolating electron conducting pathways, and stable structural integrity. Such a feasible architecture could also provide good synergism between the CNTs and the ZNC, resulting in better electrochemical performance. As a result, this nanocomposite displays impressive overall electrochemical performance. This facile and feasible method could be beneficial for preparing similar materials that require high electronic conductivity for energy storage in medical applications.

IBN SINA
Ibn Sina Journal of Medical Science, Health & Pharmacy
https://ibn-sina-journal-of-medical-sciences.jo
Vol. 2, No. 1, 2025, pp. 1-8
Ibn Sina journal Of Medical Science, Health & Pharmacy
ISSN 3104-6428

1. Introduction

Recent years have seen a significant challenge in generating clean, efficient, and renewable energy, leading to heightened scientific interest in the production, storage, and management of this valuable resource [1,2]. Supercapacitors (SCs), also known as electrochemical capacitors, have garnered significant research and commercial interest due to their extensive power storage capacity and resistance to degradation compared to other energy storage devices like batteries and fuel cells. Among these, carbon-based electrode materials, including activated carbon, carbon nanotubes, and graphene, are employed as electrode materials in electric double-layer capacitors (EDLCs). In recent times, researchers have exerted significant efforts in the pursuit of high-performance electrode materials for supercapacitors. 6,7 Currently, nanostructured mixed transition metal oxides [MTMOs] with very high specific capacitance are widely studied as potential supercapacitive electrodes [8, 9]. Significantly, studies indicate that nanostructured Zn-Ni-Co ternary oxide (ZNC) has the potential to offer more sophisticated redox reactions, demonstrate superior electrical conductivity compared to single-component transition-metal oxides with nanostructure, and provide substantial enhancements in supercapacitive properties when used as electrodes for supercapacitors [10, 11]. The comparable atomic radii of the elements make ZNC, devoid of any alteration in crystal structure, one of the most appealing materials for supercapacitive electrodes. The enhanced supercapacitive characteristic of the ZNC material is attributed to the synergistic effects resulting from the intricate chemical compositions and the many mixed valence states encountered in the multi-metal centers [12]. Experimental evidence has shown that the mixed oxide electrodes of ZNC displayMoreover, research has shown that the mixed oxide electrodes of ZNC display better electrochemical performance in comparison to the binary-component Ni-Co. This may be attributed to the combined influence of the multi-metal components and the increased oxidation states experienced by the electrodes [13]. Enhanced safety and reduced expense. Furthermore, these three metal elements may exhibit synergistic effects in the redox reaction process as compared to metal oxides consisting of just one component. Nevertheless, the limited inherent electrical conductivity and sluggish ion diffusion rates of nanostructured MTMOs generally result in low specific capacitance and/or severely inadequate cycle stability, therefore impeding their future practical usage.

One effective approach to address the aforementioned issues is to combine nanostructured mixed transition-metal oxide MTMOs with guest conducting materials. Such materials may facilitate the dispersion, reinforcement, or integration of the MTMOs. By virtue of its excellenceIt is widely believed that graphene is highly suitable for interaction with nanostructured transition metal oxides (TMO) in order to enhance the performance of electrode materials in supercapacitors [14, 15]. These characteristics are attributed to its high mechanical flexibility, extensive surface area, exceptional chemical and thermal stability, and excellent electrical conductivity. Comprehensive experiments have been conducted to examine several structural models of graphene/TMO composites and their electrochemical properties when used as electrode materials in supercapacitors [15, 16]. Also, RuO2 was used as a pseudocapacitive material with good electrochemical performance because of its high conductivity, excellent oxygen evolution, and efficient reduction reaction activity, although it has a very high cost [17]. Another promising electrode material for a supercapacitor is Co3O4, which exhibits high capacitance and good cycling performance [18]. [19] Synthesised and used mesoporous Co3O4 nanocubes as supercapacitors with a specific capacitance of 210 F g−1 at a discharge current density of 1A g−1. Bulk Co-based metal oxides often induce high toxicity, however, which limits the application of Co3O4 electrodes. So, replacing some Co atoms with many metal ions that are safe for the environment is seen as a possible way to make these oxides less harmful [20]. When introduced into Co3O4, Mn, Zn, and Ni can partially replace Co atoms, forming a ternary oxide without altering its crystal structure. This is because the atomic radii of Mn, Zn, and Ni are similar to those of Co. Mixed transition metal oxides, like MCo2O4 [M=Ni, Fe, Zn], work well because they can be in a lot of different oxidation states and are very good at conducting electricity [21,23]. [24] Proposed a straightforward technique that use a low-temperature solvothermal approach followed by calcination to produce flower-like CoMn2O4 spinel microspheres for supercapacitor electrodes. In the presence of a discharge current density of 1A g−1, they demonstrated a specific capacitance of 188 F g−1. These scientific accomplishments have enhanced the existing body of knowledge and practical use of spinel materials in supercapacitor electrodes. Wu et al. documented a straightforwardWu and colleagues provided a straightforward method for synthesising mesoporous Ni0.3Co2.7O4 hierarchical structures well-suited for supercapacitors [25]. Co2O4 nanowire cluster arrays on Ni foam for high-performance supercapacitors using simple hydrothermal and post-annealing methods in pure argon [26]. These arrays demonstrated high electrochemical performance with high specific capacitance.

Recently, three-dimensional (3D) porous Zn-Ni-Co (ZNC)-CNTs that offer various advantages, including better permeability and a large specific surface area, resulting in reactive sites, have been studied for practical applications in biomedical science, catalysis, sensors, lithium ion batteries, and supercapacitors [27,28]. Studies have demonstrated that directly growing electrode materials on conductive current collectors, such as nickel foam and carbon cloth, for supercapacitor electrodes can significantly enhance their electrochemical properties [29,30]. Three-dimensional (3D) substrate-supported hierarchical architectures are interesting because of their large surface areas, easy electrolyte access to the electrode, efficient electron transfer, fast ion transport, and good strain accommodation [31,35]. This approach not only facilitates optimal contact between the substrate and the electrode active materials, leading to a significant enhancement in ion transport, but also establishes pathways for charge transfer. These aforementioned characteristics are advantageous for optimising the use of electrochemically active materials.

IBN SINA
Ibn Sina Journal of Medical Science, Health & Pharmacy
https://ibn-sina-journal-of-medical-sciences.jo
Vol. 2, No. 1, 2025, pp. 1-8
Ibn Sina journal Of Medical Science, Health & Pharmacy
ISSN 3104-6428

Few studies have described ternary transition metal oxides as supercapacitor electrodes, despite the publication of numerous studies on binary transition metal oxides. [36] Prepared hierarchical mesoporous ZNC ternary oxide nanowire arrays successfully supported by nickel foam through a simple two-step approach: a hydrothermal method and subsequent thermal annealing. The resulting ZNC ternary oxide electrode for supercapacitors exhibited remarkable electrochemical behavior. [37] Prepared ZNC oxide nanosheets with a three-dimensional hierarchically porous architecture by growing them on Ni foam through a simple and efficient chemical bath deposition followed by thermal treatment. When used as electrodes in supercapacitors, these nanosheets exhibited high specific capacitance, outstanding rate capability, and superior cycling stability. [39] Synthesised nanostructured Mn-Ni-Co (MNC) oxide composites, and the results showed that a maximum capacitance of 1260 F g-1 could be achieved within the 0.1 to 0.4 V potential range 38. Another report by Li et al. demonstrated a facile hydrothermal method to obtain aligned spinel MNC nanowires. The resulting MNC nanowires showed a specific capacitance of 638 F g-1 at 1 A g-1 and exhibited excellent cycling stability. The electrochemical behaviour of the above ternary oxides still needs to be improved, however.

Therefore, until recently, there have been limited investigations on ZNC ternary oxides and their use in supercapacitors. If compared to pure Co3O4 electrode materials, the ZNC electrode materials would significantly lower the cost and exhibit superior safety performance simultaneously. We anticipate that ZNC electrode materials, including cobalt, nickel, and zinc ions, will have a synergistic impact on redox processes relative to their individual single-component oxides. This phenomenon arises from the fact that nickel (Ni) has a high capacity and can enhance the density, conductivity, and roughness of active sites; cobalt (Co) provides higher electronic conductivity; and zinc (Zn) exhibits excellent electrical conductivity, leading to superior electrical conductivity and capacitive performance [40,41]. Moreover, the incorporation of several metal ions may yield multiphase metal oxides and introduce abundant structural defects. This approach can also improve the stability and cycle life of the metal oxide electrode. Furthermore, the electrochemical activity of ternary transition metal oxides is higher, and their electronic conductivities are stronger than those of binary transition metal oxides, so that the former is more favourable than the latter for applications in high-performance electrochemical energy storage [41]. The introduction of CNTs resulted in increased conductivity and surface area of ZNC. In addition, the lightweight but free-standing CNTs were able to wrap the ZNC hexagonal nanoplates, so that a relatively high mass loading of CNTs on ZNC was easily attained. To improve the electrochemical performance of ZNC materials at high rates, it is critical to develop electrodes with a large number of electroactive sites and to enhance the transport of ions and electrons in the electrodes as well as on the electrode-electrolyte interface. Based on the considerations above, great efforts have been made to grow electroactive nanostructures on conductive substrates to be directly used as integrated electrodes for supercapacitors [42–44]. CNTs are generally regarded as promising candidates for high-performance electrodes due to their excellent conductivity, high specific surface area, and high thermal and chemical stability [45, 46]. Therefore, the ZNC-CNT hexagonal nanoplates exhibit high specific capacitance and excellent cycling stability. The material assembly procedure and a schematic illustration of the ternary electrode are shown in Figure 1.

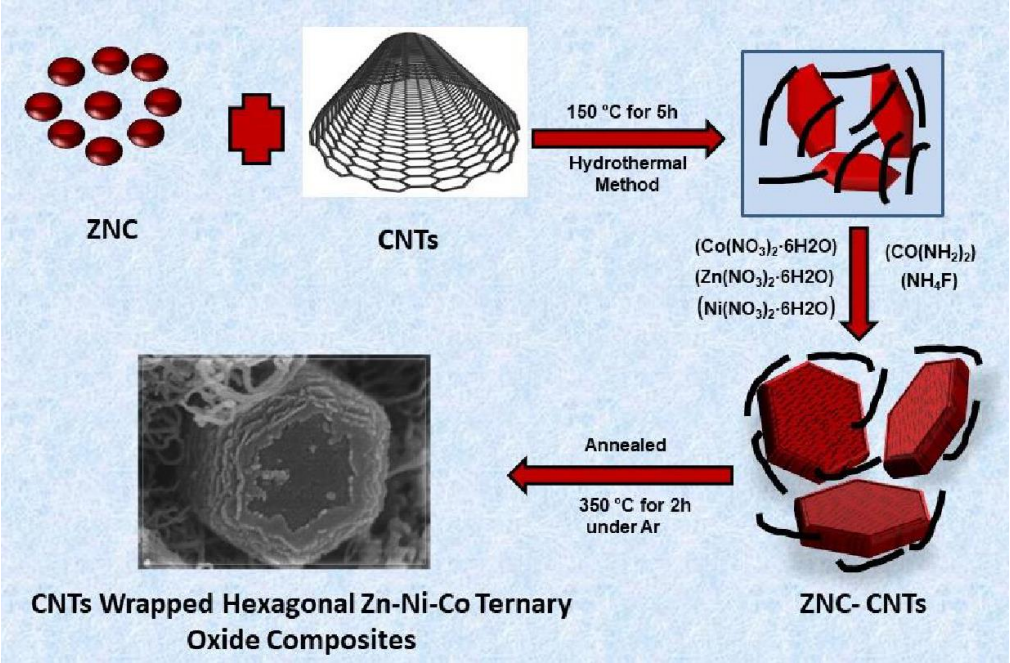

Figure 1: Schematic illustration of the preparation steps for ZNC–CNTs nanocomposite.

Herein, we report a facile and environment friendly strategy to prepare 3D nickel foam supported porous ZNC-CNTs hexagonal nanoplate arrays and investigated their physical and electrochemical characteristics as binder-free electrode material for supercapacitors. The ZNC-CNTs electrodes yielded a high specific capacitance of 2360 Fg^{-1} at a discharge current density of 2 Ag^{-1} and exhibited good cycling stability. In this nanostructure, the CNTs not only act as a current substrate for the ZNC, but also significantly increase the surface area and dramatically accelerate ion diffusion because of their low energy barriers. Applied as electrode materials for supercapacitors, this nanostructured ZNC-CNTs electrode has appealing rate capability, high specific capacity, and excellent cycling characteristic. The very high specific capacitance, great rate capability, and remarkable cycle stability of nickel foam supported porous ZNC-CNTs hexagonal nanoplate arrays make them highly appealing and viable candidates for supercapacitor electrodes.

EXPERIMENTAL SECTION

Synthesis of Carbon Nanotubes (CNTs)

The initial CNTs were fabricated by the chemical vapor deposition (CVD) method [47,48]. The prepared CNTs were immersed in mixed acid with a volume ratio of 3:1 of H2SO4 (98%) to HNO3 (65%) for 12 h, followed by washing to neutral pH and drying. All other chemicals used in the present study were of analytical grade, purchased from Sigma Aldrich, and used without further purification.

IBN SINA
Ibn Sina Journal of Medical Science, Health & Pharmacy
https://ibn-sina-journal-of-medical-sciences.jo
Vol. 2, No. 1, 2025, pp. 1-8
Ibn Sina journal Of Medical Science, Health & Pharmacy
ISSN 3104-6428

PREPARATION OF ZNC-CNTS NANOCOMPOSITE.

The ZNC-CNTs nanocomposite was synthesized by a hydrothermal method. The synthesis involved the following steps: Different proportions of CNTs (13, 16, 18, 20, 22, and 24 mg) were dispersed in 40 ml distilled water using ultra-sonication for a period of 30 min. Then, 1.74 g of cobalt nitrate hexahydrate (Co(NO3)2·6H2O), 0.892 g of zinc nitrate hexahydrate Zn(NO3)2·6H2O, 0.872 g of nickel nitrate hexahydrate (Ni(NO3)2·6H2O), 0.720 g of urea (CO(NH2)2), and 0.148 g of ammonium fluoride (NH4F) were mixed with 80 mL of deionised (DI) water. The reaction mixture and put into a 100 mL Teflon-lined stainless-steel autoclave and kept at 150℃ for 5 h. After the autoclave was cooled down to room temperature, the samples were washed using an ultrasonic bath several times and dried at 80 °C for 12 h. Finally, the obtained samples were put into a programmable furnace and annealed at 350 °C under Ar atmosphere with a ramping rate of 2 ºC min-1 to obtain the final product, which is ZNC-CNTs composite. Pristine ZNC was prepared by the same method without adding CNTs.

2. Materials and Method

The morphology of the ZNC and ZNC-CNTs was determined using high resolution transmission electron microscopy (HRTEM; JEOL JEM-2011) and scanning electron microscopy (SEM; JEOL JSM-7500FA). Phase analyses were carried out using X-ray diffraction (XRD; GBC MMA XRD), Raman spectroscopy (JY HR800 Spectrometer), and Fourier transform infrared (FTIR) spectroscopy (Shimadzu FTIR Prestige-21). Surface area was measured using a Brunauer-Emmett-Teller (BET) analyzer (Nova 1000). Pore size distributions were calculated using the non-local density functional theory (NLDFT) slit-cylinder pore equilibrium model for N2 at 77 K, as implemented in the Quantachrome software (v 3.0).

ELECTROCHEMICAL MEASUREMENT

The working electrode was fabricated by applying a uniform mixture of ternary metal oxide, acetylene black, and polyvinylidene fluoride in a weight ratio of 8:1:1 in N-methyl-2-pyrrolidone over 1.0× 2.0 cm2 Ni foam pieces specifically designed for current collecting. The electrode was then thoroughly dried at 120°C under vacuum conditions. The blended products were immediately applied to the nickel foam current collector as a working electrode and then compressed to a thin foil at a pressure of 10 MPa before to each test. The mass of the active substance put on each electrode was measured to be between 0.86 and 1.0 mg using a microbalance (Sartorius, BS124S) with a precision of 0.1 mg. All electrochemical quantifications were conducted in a 2 M KOH aqueous solution using a conventional three-electrode setup. An active material-loaded Ni foam, platinum foil, and Hg/HgO electrode were used as the working electrode, counter electrode, and reference electrode, respectively. An electrochemical workstation (CHI660B, Chenhua, Shanghai) was used to conduct cyclic voltammetry (CV) experiments across the potential range of 0−0.55 V (vs. Hg/HgO) at various scan speeds. The galvanostatic charge-discharge (GCD) experiments were performed using a test configuration controlled by a LAND battery software. Electrochemical impedance spectroscopy (EIS) using a CHI660B instrument was conducted by delivering a 5 mV amplitude AC voltage throughout a frequency range of 0.01 Hz to 100 kHz assuming an open circuit potential.

3. Results and Discussion

STRUCTURE AND MORPHOLOGY

The phases of the as-prepared samples were first determined from XRD patterns of CNT, ZNC, and the ZNC-CNT nanocomposite, as shown in Fig. 2 The XRD pattern of pristine CNT shows two diffraction peaks at 26.5° and 43.5° which can be indexed to the (002) and (101) planes, respectively 49,50. All XRD diffraction peaks of the as-prepared ZNC electrode materials can be indexed as the spinel structured phase of the space group Fd3m (JCPDF Card:74-2120). The thermal stability of the ZNC and ZNC-CNTs composites in air was examined by thermogravimetric analysis (TGA). Figure SI-I in the Supporting Information shows a comparison of the weight loss of pristine ZNC and the different ratio for the ZNC-CNTs nanocomposites. All ZNC-CNTs samples were heated from room temperature to 850 °C under normal atmosphere at a

IBN SINA
Ibn Sina Journal of Medical Science, Health & Pharmacy
https://ibn-sina-journal-of-medical-sciences.jo
Vol. 2, No. 1, 2025, pp. 1-8
Ibn Sina journal Of Medical Science, Health & Pharmacy
ISSN 3104-6428

ramping rate of 10 °C min-1. The weight loss around 450°C was due to the oxidation of carbon. From this, the weight percentages of CNTs in different ratios were observed to be 0, 13, 18, 20, 22, and 24 wt%. According to the wt% of CNTs in the ZNC-CNTs composites, the samples were designated as ZNC, ZNC-13CNTs, ZNC-16CNTs, ZNC-18CNTs, ZNC-20CNTs, ZNC-22CNTs and ZNC-24CNTs. The morphology, size, and nanostructure of the samples were investigated by SEM, TEM, and high-resolution TEM (HRTEM). The morphologies of the as-prepared samples were investigated by field emission SEM (FESEM). Figure. 3(a-f) shows the SEM images of the ZNC-CNTs composites with different wt% of CNTs. The ZNC-CNTs exhibit a hexagonal plate like morphology with lateral sizes of 400–600 nm and thickness of 200-250 nm. As can be seen, numerous CNTs were found to be well-dispersed around the hexagonal plates to form a composite structure. This CNT wrapped ZNC network possesses the following advantages: 1) The CNTs work as charge carrier transport channels, making the composite conductive in nature; 2) it provides electroactive sites for the redox reactions; 3) it effectively prevents the agglomeration of ZNC hexagon plates and ensures maximum utilization of the electroactive materials; and 4) it reduces the volume changes of the electrode materials during the charge-discharge reaction [51,52]. In short, this network plays an important role in improving the conductivity and stability of the electrode systems.

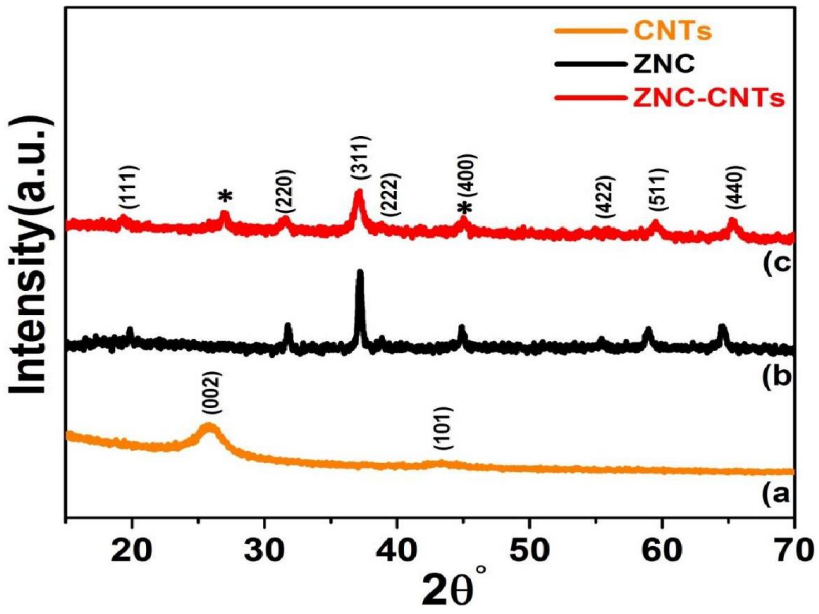

Figure 2: (a) XRD patterns of a CNTs, b) pristine ZNC, c) ZNC-CNTs hexagonal nanoplates composite.

The FESEM images (Figure. 3(a, b)) of the pristine ZNC demonstrate the hexagon morphology with diameters of about 400-630 nm and thickness of about 50-120 nm. Figure 3(c) shows a TEM image and Figure.3(d) presents the corresponding selected area electron diffraction (SAED) pattern, which reveals the crystalline nature of the ZNC hexagonal plates. Figure. 3 (a, b) shows FESEM images of CNTs at different magnifications, which demonstrate the uniformity of the CNTs used in the present study. The TEM images, as shown in Figure. 3 (c, d), demonstrate the hollow nature of the CNTs. The inner diameters of the CNTs are observed to be in the range of 30 to 40 nm, and the wall thickness ranges from 1.5 to 4.5 nm. The selected area electron diffraction (SAED) pattern in (Figure. 3 (e)) presents bright electron diffraction spots in the Debye ring, corresponding to the d spacing of 0.338 nm for the (002) lattice planes.

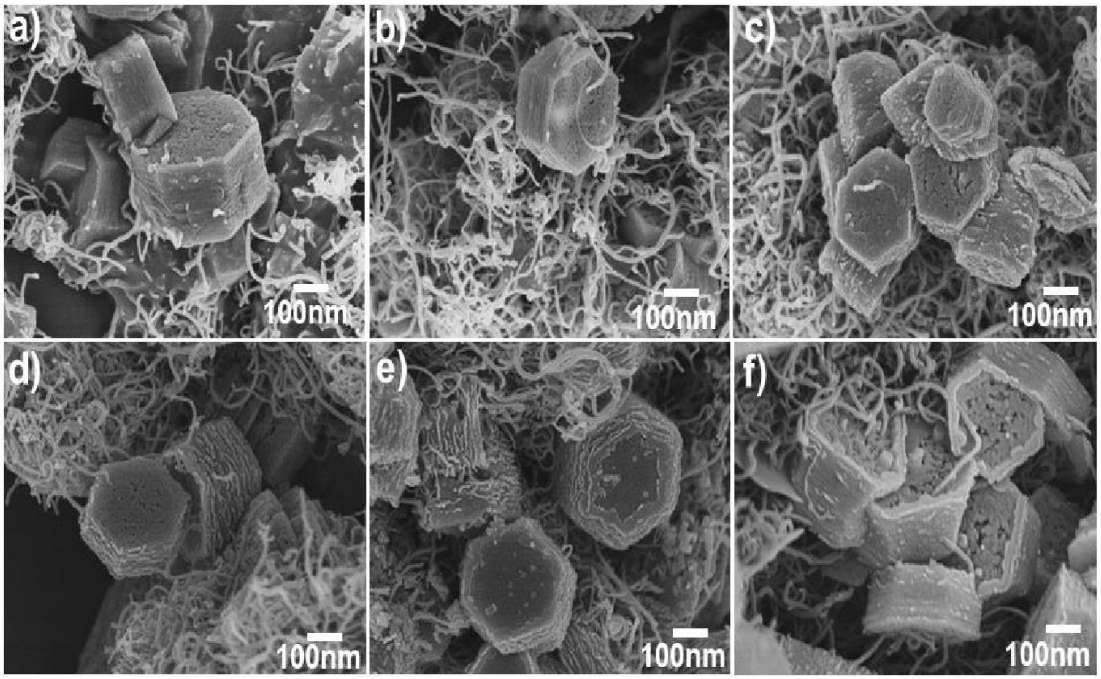

Figure 3: FESEM images of a) ZNC–13mg CNTs, b) ZNC-16mg CNTs, c) ZNC-18mg CNTs, d) ZNC-20mg CNTs, e) ZNC-22mg and f) ZNC-24mg CNTs hexagonal nanoplate composites.

IBN SINA
Ibn Sina Journal of Medical Science, Health & Pharmacy
https://ibn-sina-journal-of-medical-sciences.jo
Vol. 2, No. 1, 2025, pp. 1-8
Ibn Sina journal Of Medical Science, Health & Pharmacy
ISSN 3104-6428

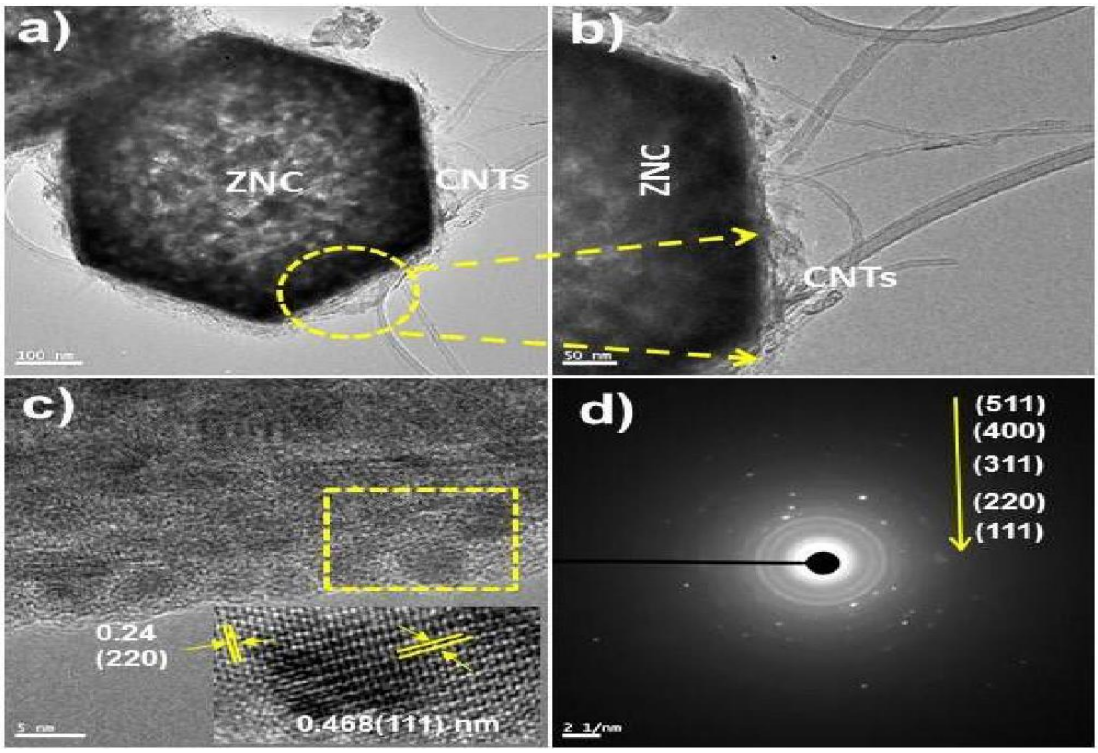

Figure 4. (a-c) TEM images of ZNC-22CNTs, (d, e) HRTEM images showing the lattice fringes of ZNC-22CNTs, and f) the corresponding SAED pattern

Figure 4 (a-d) represent different magnified TEM images of ZNC-22CNTs nanocomposite. The diameters of these hexagon plates are observed to be 400-625 nm. The HRTEM images in Figure. 4(c) show the lattice fringes with spacing of 0.24 and 0.468 nm, corresponding to the (220) and (111) planes. SAED pattern in Figure 4 (d) demonstrates polycrystalline nature of the sample. The SAED patterns are composed of well-defined rings, and this diffraction rings can be readily indexed to the (111), (220), (311), (440), and (511) planes of porous ZNC. From the SEM and TEM images of ZNC-22CNTs structure, it should be noted that the CNTs are well wrapped around the ZNC. Thus, this composite is considered to be electrochemically more active as compared to the pristine ZNC counterpart. This CNT coating could be beneficial for easy access of ions and electrons to the active surfaces, consequently enabling fast conversion reactions and resulting in better power performance. Also, since the CNTs can work as a mechanical buffer, a large change in the volume of ZNC can be accommodated without particle isolation from the CNTs, leading to improved cycling performance Figure. SI-IV presents a TEM image of the ZNC and elemental mapping of pristine ZNC, which demonstrates the presence of zinc, nickel, cobalt, and oxygen. By comparing the energy dispersive spectroscopy (EDS) mappings of pristine ZNC (Figure 5) and

ZNC-22CNTs (Figure 6), the ZNC-22CNTs system clearly shows the presence of a well wrapped CNT coating.

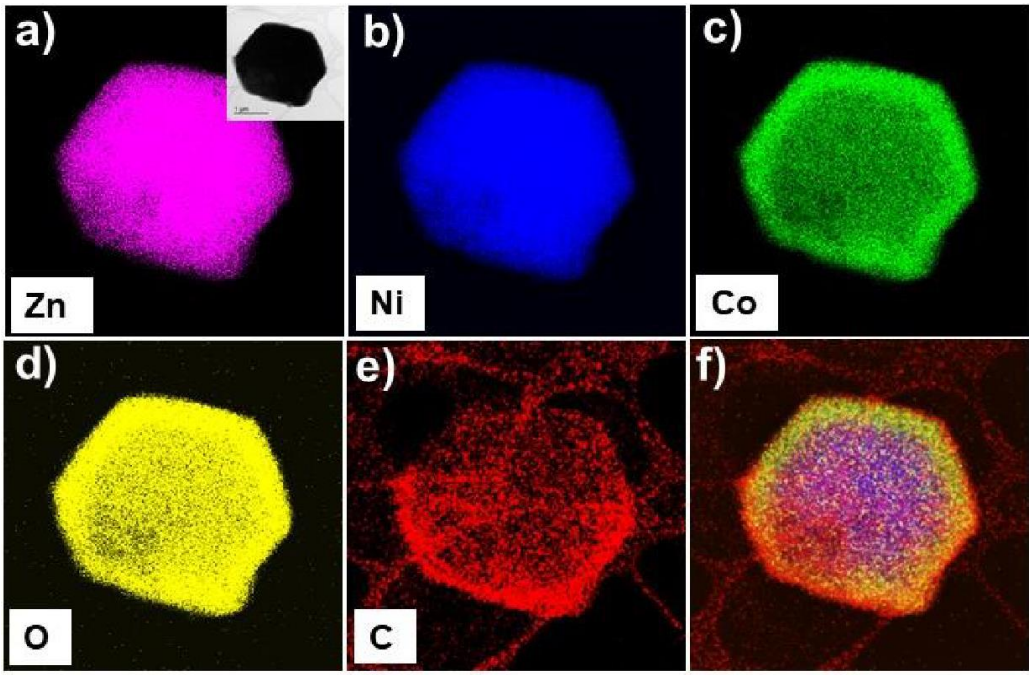

Figure 5: Elemental mapping of ZNC-22CNTs showing the presence of (a) Zinc (inset: TEM image of ZNC-22CNTs) (b) Nickel, (c) Cobalt, (d) Oxygen, (e) Carbon, (f) combined Zn, Ni, Co, O, and C mapping of the ZNC-22CNTs composite.

The BET and BJH testing were performed to evaluate the specific surface area and pore-size distribution of the CNTs, ZNC and ZNC-CNTs composite (Figure 5) From the profiles, the specific surface areas of the CNTs, ZNC, and ZNC- 22CNTs were calculated to be 228.467, 154.789, and 205.974 m2g-1, respectively. The improved surface area of the composite sample as compared to the pristine ZNC is beneficial in terms of providing more active electrode surface for the redox reaction, which we believe to be very crucial for the better electrochemical performance of a supercpacitor electrode. Important parameters were derived from the BET and BJH studies and are tabulated in Table SI.

Raman spectroscopy plays a critical role in the characterization of materials, and it was employed in this study to gain information on the CNTs in the composite materials. Figure 5 (a) shows the Raman spectra of the ZNC and ZNC-22CNTs composite. For ZNC- 22CNTs the peaks observed at

Vol. 2, No. 1, 2025, pp. 1-8
ISSN 3104-6428

1327.5, 1594.2, and 2648 cm−1 clearly demonstrating D, G, and 2D band of CNTs, respectively, whereas the peaks at 471.8, 516.3, and 668.7 cm-1 belong to the

Eg, F2g and A1g modes of ZNC Figure 5 .(b) demonstrate the Fourier transform infrared (FT-IR) spectroscopy study in the range of 4000–500 cm−1 of ZNC and ZNC-22CNTs nanocomposite. The identified peaks at 806.1, 1010, 2384, and 3498 cm-1 represents different vibrations of C-O, C=C, C-H, and O=H bonds. The presence of additional peaks at 1627 and 1990.5 cm-1 for ZNC-22CNTS, represent the linking of the oxygenated functional groups in the ZNC53 resulted from infrared (IR) absorption by each of these bonds at various frequencies, which possibly occurred due to the lattice strain arising from the mismatch in the coefficient of thermal expansion between the ZNC and the CNT during the synthesis [54].

The electrochemical performance of electrode systems can be determined using different techniques, including cyclic voltammetry (CV), galvanostatic charge/discharge (GCD) curves, and electrochemical impedance spectroscopy (EIS) using a three-electrode system. To find out the optimal CNT concentration in the ZNC-CNTs composites, different electrochemical performance tests were carried out (Figure 6). Figure 6 (a) presents the CV curves of the ZNC and different ZNC-CNTs composites at a scan rate of 2 mVs-1. A pair of redox peaks was observed in all the CV curves, which demonstrates the typical pseudocapacitance performance. The specific capacitance values of ZNC, ZNC-13CNTs, ZNC-16CNTs, ZNC-18CNTs, ZNC-20CNTs, ZNC-22CNTs and ZNC-24CNTs were calculated to be 1233, 1380,1665, 1832, 1998, 2188 and 2165 Fg-1, respectively, from the CV curves (Fig. 6(a)). Figure 6 (b) shows the specific capacitance variation as a function of CNT content. It is shown that, as the content of CNTs increased, the ZNC-CNTs system showed an improvement in the specific capacitance. The reason for this improvement could be attributed to a) the effective charge collection, b) the reduced diffusion length, and c) the improved BET active surface area, provided by the CNTs in the ZNC-CNTs composite system.

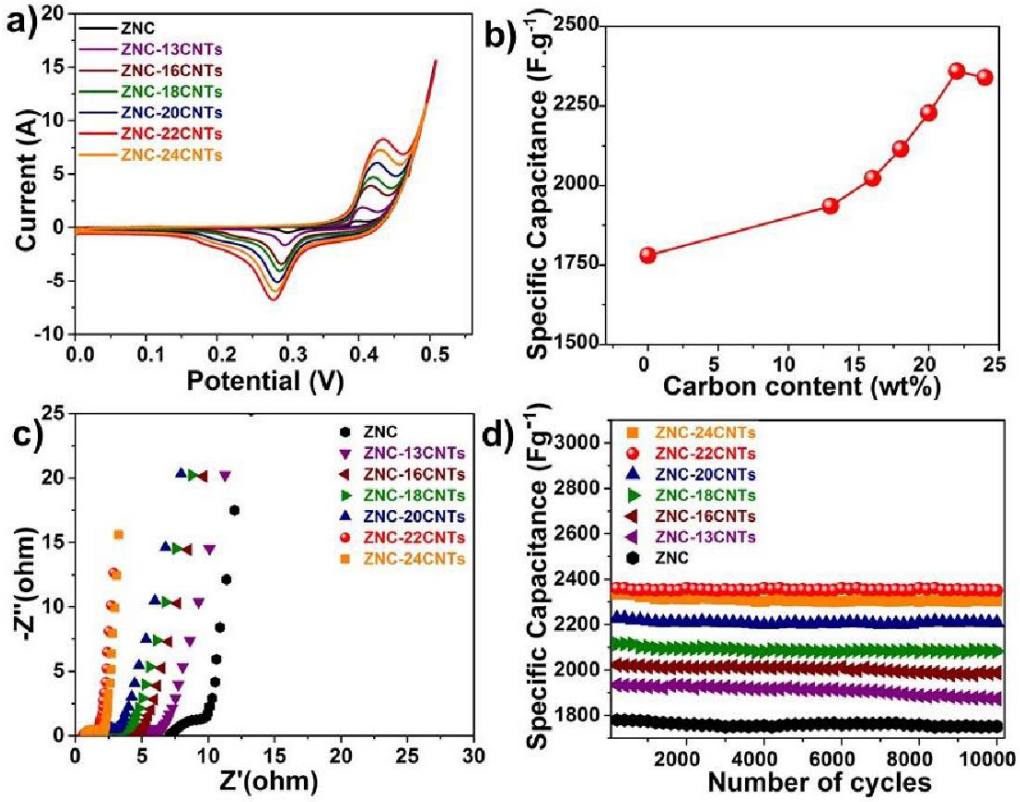

Figure 6. a) CV curves of ZNC arrays for various CNT to ZNC ratios, b) specific capacitance vs. carbon content plot, c) Nyquist plots recorded between 1 Hz and 100 kHz, and d) cycling performance of ZNC-CNTs hexagonal nanoplates composite for various CNT to ZNC ratios.

Furthermore, EIS analysis (Figure 6(c)**)** and cycling performance studies (Figure 6(d)) were also carried out to find the optimal electrode. By considering all the electrochemical characterizations, the best performing electrode was observed to be ZNC-22CNTs. Figure. 7 (a, b) shows the CV curves of the ZNC-22CNTs composite and ZNC samples at different scan rates. A pair of redox peaks could be found in each CV curve, which represents the reversible reactions of Zn2+/Zn3+, Co3+/Co2+, and Ni3+/Ni2+. The specific capacitances for ZNC-22CNTs were found to be 2118, 1778, 1590, 1270, 1106, 1052, and 1006 Fg^{-1} at scan rates of 1, 5, 10, 20, 30, 50 and 100 mV s-1, respectively, On the other hand, the specific capacitance values for the pristine ZNC electrode at the same scan rates are observed to be 1220, 1256, 1134, 1106, 988, 864 and 702 $F{\cdot}g^{-1}$. So, the capacitance values for ZNC-22CNTs were found to be much higher as compared to the pristine ZNC sample at all scan rates. This result further confirms that the ZNC-22CNTs electrode possesses great storage capacity and a high rate capability. Further, GCD measurements were carried out at various current densities from 2 Ag-1 to 8 Ag^{-1} (Figure 7(c, d)). The corresponding

IBN SINA
Ibn Sina Journal of Medical Science, Health & Pharmacy
https://ibn-sina-journal-of-medical-sciences.jo
Vol. 2, No. 1, 2025, pp. 1-8
ISSN 3104-6428

specific capacitances of the ZNC-22CNTs electrode were calculated to be 2276, 2216, 2183 and 1866 F·g-1 at different current densities of 2, 4, 6, and 8 Ag-1, respectively. The capacitance values obtained for the pristine ZNC samples were 1680, 1414, 1375, and 1012 $F \cdot g^{-1}$ at current densities of 2, 4, 6, and 8 $A.g^{-1}$ respectively. This further demonstrates that the ZNC-22CNTs electrode shows better storage capability and higher rate performance. Also, we believe that the interactions and synergism between ZNC and CNTs promote fast electron transport, resulting in strong redox features of Zn2+Zn3+, Co2+Co3+, and Ni2+Ni3+ in the ZNC-CNTs composite. In both cases, the specific capacitance reduction with increasing scan rate or current could be attributed to low entry of the electrolyte into the electrode bulk and/or insufficient time to complete the redox reactions. This suggests that ZNC-22CNTs has better electrochemical activity as compared to the pristine ZNC sample. This better electrochemical performance could be attributed to its high surface area and the improved electronic conductivity provided by the CNTs in the ZNC-22CNT composite system.

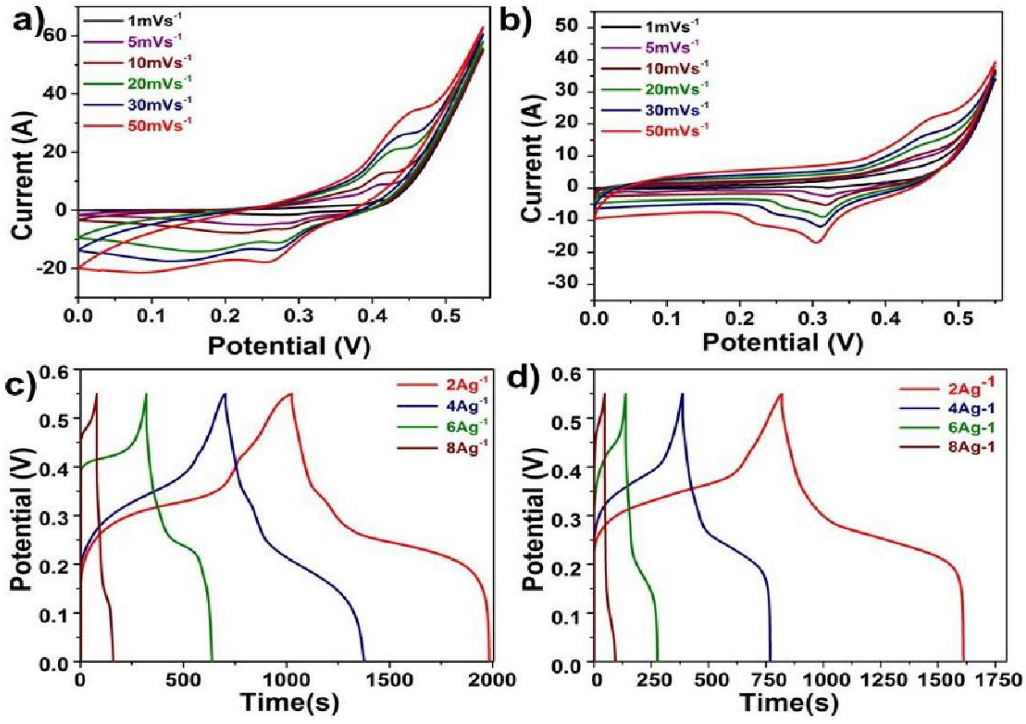

Figure 7: a CV curves at different scan rates of ZNC-22CNTs hexagonal nanoplate composite, b) CV curves of ZNC at different scan rates, c) charge/discharge curves at different current densities of ZNC-22CNTs hexagonal nanoplates, and d) charge/discharge curves of ZNC at different current densities.

Further, to have the effect of CNTs on the ZNC, we have carried out the one to one comparison of the electrochemical performance of pristine ZNC and ZNC-22CNTs composites. CV and GCD were conducted using three-electrode mode in 2 M KOH solution. Figure 8 (a) presents the CV curves of supercapacitor electrodes prepared from both ZNC-22CNTs hexagonal nanoplates and pristine ZNC at 2 mVs^{-1} scan rate in the potential range of 0.0 to 0.55 V (vs. Hg/HgO). The GCD curves of ZNC and ZNC-22CNTs at 2 Ag-1 current are shown in Figure 8 (b). These curves also demonstrate the pseudocapacitance of ZNC-22CNTs composite and ZNC. By comparing the capacitance values of ZNC (CV: 1220 F g^{-1} and GCD: 1680 F g^{-1}) and ZNC-22CNTs (CV: 2118 F g^{-1} and GCD: 2276 F g^{-1}), the far superiority of the composite sample over pristine ZNC is clearly evident. Figure 8(c) shows the Nyquist plots for the electrodes recorded from 0.01 Hz to 100 kHz. The linear region in the lower frequency range is indicative of capacitive behavior of the electrodes. The decrease in the solution resistance (Rs) value for the ZNCO-22CNTs (0.21 Ω) as compared to pure ZNC (7.3 Ω) could be due to the enhanced electronic conductivity of ZNC-22CNTs provided by the CNTs. This lower Rs value could be favourable in terms of better power performance 37-43. The smaller semicircle, indicating a smaller charge transfer resistance (*R*ct) for ZNC-22CNTs (2.5 Ω) as compared to ZNC (10Ω), demonstrates the lower electrochemical resistance of the composite system compared to the pristine sample. Figure 8 (d) shows the cycling stability curves of ZNC-22CNTs and pristine ZNC electrodes at a current density of 2 A g^{-1}. The ZNC-22CNTs composite system showed excellent cycling performance with ~96% capacitance retention for 10000 consecutive charge/discharge cycles. The pristine ZNC sample, however, could only retain 90% of its initial capacitance at the end of 10000 cycles at the same current density. This improved cycling performance could be attributed to the synergism between the ZNC and CNTs and the CNTs ability to reduce the volume changes of the electrode materials during the charge-discharge reaction. The results discussed above clearly confirm that the ZNC-CNTs hexagonal nanoplates have excellent specific capacitance and energy performance with good power density, which could be deduced from the following factors. Firstly, by using a conductive support of CNTs, ZNC can be well dispersed over a large area, by effectively preventing agglomeration and thus ensuring the maximum utilization of active electrode materials. Secondly, these CNTs could provide double-layer capacitance. Furthermore, the use of high surface area carbon nanotubes (CNTs) might enhance the specific surface area of the hybrid material. Finally, carbon nanotubes (CNTs) possess exceptional conductivity and mechanical characteristics together with commendable stability. Therefore, the presence of these individual carbon nanotubes (CNTs) in the electrode created a three-dimensional conductive network. This network enhanced the electrical

conductivity of the electrode and facilitated the movement of electrons and ions within the bulk electrode material. Additionally, it ensured improved stability during charge/discharge cycles.

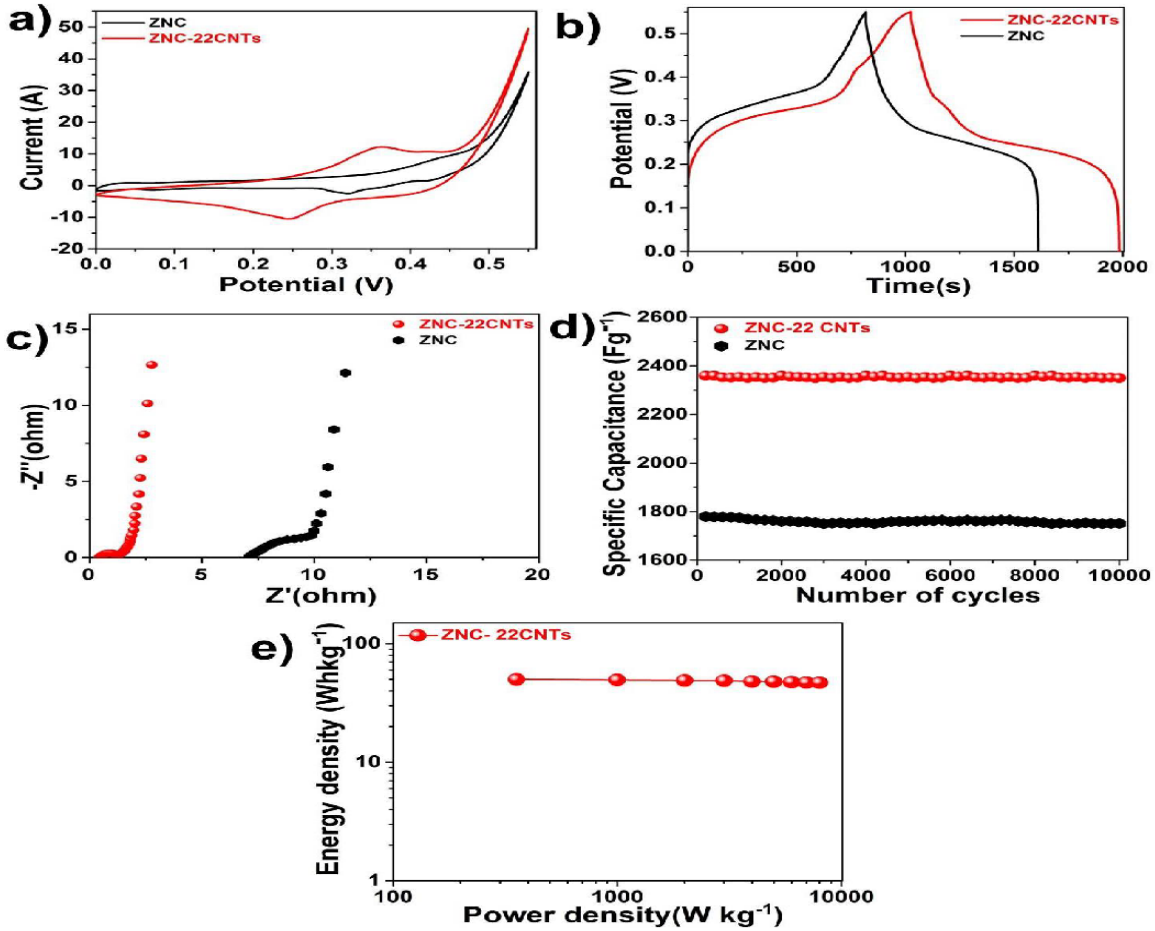

Figure 8: a) CV curves of the ZNC and ZNC-22CNTs, b) charge/discharge curves of ZNC and ZNC-22CNTs hexagonal nanoplate composite, c) electrochemical impedance spectra, d) cycling performances of ZNC and ZNC-22CNTs hexagonal nanoplate ,and e) Ragone plot of the ZNC- 22CNTs nanocomposite.

Energy density and power density are the two important factors to evaluate the practical applications of supercapacitors; these have been obtained using the following two equations 56,59.

$E = 1/2 \times C \times (\Delta V)\ 2$ (1)

$P = E/\Delta t$ (2)

Where C is the mass capacitance of the supercapacitor, E represents the energy density, P denotes the power density, ΔV is the potential drop during the discharge process, and Δt is the discharging time.

Figuer 8 presents the Ragone plot of the ZNC-22CNTs supercapacitor device. The device showed highest energy density of ~50 W h kg^{-1} at a power density of 355 W kg^{-1}. Compared with the other reported values37,38,57,58,61.62The composite system in the present work showed better results, which makes the ZNC-22CNTs composite device a promising candidate for future energy storage.

4. Conclusion

In summary, ZNC-CNTs hexagonal nanoplates were synthesized by a facile two-step approach involving a hydrothermal method followed by calcination process. This composite material demonstrated a high capacitance value of 2360 F g-1 at 2 A g−1 and an excellent cycling performance with ~96% capacitance retention, even at the end of 10000 cycles. The ZNC-CNTs nanocomposite showed a power density of 355 W kg-1 and a maximum energy density of 50 WH kg-1, respectively. Furthermore, the introduction of CNTs to wrap the ZNC hexagonal nanoplate resulted in great advantages, such as increases in conductivity, stability and surface area. The combined impacts of carbon nanotubes (CNTs) and zinc nanocoils (ZNC) are accountable for the exceptional characteristics of the composite system, such as outstanding capacitance, high power efficiency, and strong cycle stability. The exceptional characteristics of this ZNC-22CNTs composite render it a promising contender for use as an electrode material in supercapacitor devices. Furthermore, the simple and practical material production method used in this work may be readily expanded to the fabrication of various composites based on ternary oxides with regulated structure.

5. References

[1] Miller, J. R.; Simon, P. Electrochemical capabilities of nanomaterials for energy storage. Science 2008, 321(5194), 651-653. https://doi.org/10.1126/science.1158736

[2] Chmiola, J.; Largeot, C.; Taberna, P. L.; Simon, P.; Gogotsi, Y. Monolithic carbide-derived carbon films for micro-supercapacitors. Science 2010, 328(5977), 480-484. https://doi.org/10.1126/science.1184126

[3] Simon, P.; Gogotsi, Y. Materials for electrochemical capacitors. Nature Materials 2008, 7(11), 845-854. https://doi.org/10.1038/nmat2297

[4] Guo, G.; Huang, L.; Chang, Q.; Ji, L.; Liu, Y.; Xie, Y.; Shi, W.; Jia, N. Growth of large-area graphene on Pt foils. Applied Physics Letters 2011, 99(8), 083111. https://doi.org/10.1063/1.3626061

[5] Wang, G.; Zhang, L.; Zhang, J. A review of electrode materials for electrochemical supercapacitors. Chemical Society Reviews 2012, 41(3), 797-828. https://doi.org/10.1039/c1cs15060j

[6] Byeon, A.; Glushenkov, A. M.; Anasori, B.; Urbankowski, P.; Li, J.; Byles, B. W.; Blake, B.; Van Aken, K. L.; Kota, S.; Pomerantseva, E.; Lee, J. W.; Chen, Y.; Gogotsi, Y. Three-dimensional graphenes for supercapacitor electrodes. Journal of Power Sources 2016, 326, 686-694. https://doi.org/10.1016/j.jpowsour.2016.07.020

[7] Du, H.; Yang, H.; Huang, C.; He, J.; Liu, H.; Li, Y. Nanostructured conductive polymer hydrogels for high-performance supercapacitors. Nano Energy 2016, 22, 615-622. https://doi.org/10.1016/j.nanoen.2016.02.038

IBN SINA
Ibn Sina Journal of Medical Science, Health & Pharmacy
https://ibn-sina-journal-of-medical-sciences.jo
Vol. 2, No. 1, 2025, pp. 1-8
Ibn Sina journal Of Medical Science, Health & Pharmacy
ISSN 3104-6428

[8] Tang, Q.; Chen, M.; Wang, L.; Wang, G. Graphene-based materials in electrochemical capacitor applications. Journal of Power Sources 2015, 273, 650-662. https://doi.org/10.1016/j.jpowsour.2014.09.112

[9] Kong, D.; Ren, W.; Cheng, Y.; Wang, Y.; Huang, Z.; Yang, H. Y. Graphene-wrapped Fe3O4 anode material with improved reversible capacity and cyclic stability for lithium ion batteries. ACS Applied Materials & Interfaces 2015, 7(30), 21334-21346. https://doi.org/10.1021/acsami.5b05914

[10] Yin, C.; Yang, C.; Jiang, M.; Deng, C.; Yang, L.; Li, J. High-performance supercapacitors based on reduced graphene oxide in aqueous and ionic liquid electrolytes. ACS Applied Materials & Interfaces 2016, 8(32), 2741-2752. https://doi.org/10.1021/acsami.5b11727

[11] Yin, B. S.; Wang, Z. B.; Zhang, S. W.; Chang, L.; Ren, Q. Q. Electrochemical characterization of activated graphene materials for supercapacitors. ACS Applied Materials & Interfaces 2016, 8(30), 26019-26029. https://doi.org/10.1021/acsami.6b05815

[12] Yuan, C.; Wu, H. B.; Xie, Y.; Lou, X. W. Hybrid silicon anode materials for lithium-ion batteries. Angewandte Chemie International Edition 2014, 53(12), 1488-1504. https://doi.org/10.1002/anie.201308719

[13] Zhang, Q.; Zhao, B.; Wang, J.; Chong, Q.; Sun, H.; Zhang, K.; Liu, M. Three-dimensional porous graphene-based materials for high-performance electrochemical supercapacitors. Nano Energy 2016, 28, 475-485. https://doi.org/10.1016/j.nanoen.2016.08.023

[14] Kumar, N. A.; Baek, J. B. Metal oxides and oxychlorides for energy storage applications: a review. Nanotechnology 2015, 26(49), 492001. https://doi.org/10.1088/0957-4484/26/49/492001

[15] Kumar, R.; Singh, R. K.; Dubey, P. K.; Singh, D. P.; Yadav, R. M. Nitrogen-doped graphene for energy storage applications: advances and challenges. ACS Applied Materials & Interfaces 2015, 7(28), 15042-15052. https://doi.org/10.1021/acsami.5b02507

[16] Zhang, C.; Kuila, T.; Kim, N. H.; Lee, S. H.; Lee, J. H. Chemical functionalization of graphene and its applications. Carbon 2015, 89, 326-357. https://doi.org/10.1016/j.carbon.2015.03.014

[17] Mohamed, S. G.; Tsai, Y. Q.; Chen, C. J.; Tsai, Y. T.; Hung, T. F.; Chang, W. S.; Liu, R. S. Graphene/multiwall carbon nanotube composite film for supercapacitor application. ACS Applied Materials & Interfaces 2015, 7(30), 12038-12049. https://doi.org/10.1021/acsami.5b03483

[18] Wang, H. Z.; Shi, Y. L.; Li, Z. X.; Zhang, W. G.; Yao, S. W. A review on electrode materials for electrochemical supercapacitors. Chemistry Research 2014, 30(8), 650-654. https://doi.org/10.1007/s40643-014-0017-1

[19] Liu, X. M.; Long, Q.; Jiang, C. H.; Zhan, B. B.; Li, C.; Liu, S. J.; Zhao, Q.; Huang, W.; Dong, X. C. Graphene-based electrodes for supercapacitors. Nanoscale 2013, 5(23), 6525-6531. https://doi.org/10.1039/c3nr02021a

[20] Zhang, G. Q.; Lou, X. W. Hollow structured materials for electrochemical energy storage applications. Advanced Materials 2013, 25(7), 976-979. https://doi.org/10.1002/adma.201204484

[21] Hassan, Z., et al., "Determination antimicrobial activity of leaves extracted by various solvents from (Elephantopus scaber L.)." In IOP Conference Series: Materials Science and Engineering, vol. 454, no. 1, p. 012110. IOP Publishing, 2018, DOI 10.1088/1757-899X/454/1/012110.

[22] Guo, L. Y.; Ru, Q.; Song, X.; Hu, S. J.; Mo, Y. D. Efficient synthesis of hybrid nanocomposites as anode materials for lithium-ion batteries. RSC Advances 2015, 5(30), 19241-19248. https://doi.org/10.1039/c5ra00199k

[23] Zhu, B. G.; Tang, S. C.; Xie, H.; Zhu, J.; Meng, X. K. Facile synthesis of MoS2/C nanocomposites as high-performance anode materials for lithium-ion batteries. Chemical Communications 2016, 52(14), 2624-2627. https://doi.org/10.1039/c5cc10335e

[24] Ren, L.; Chen, J.; Wang, X. Q.; Zhi, M. J.; Wu, J. W.; Zhang, X. H. Hierarchical porous carbon nanosheets derived from waste pomelo peel for high-performance supercapacitors. RSC Advances 2015, 5(39), 30963-30969. https://doi.org/10.1039/c5ra03818e

[25] Wu, H. B.; Hao, P.; Lou, X. W. Iron carbide nanoparticles encapsulated in mesoporous Fe-N-doped carbon nanofibers for efficient electrocatalysis. Energy & Environmental Science 2013, 6(12), 3619-3623. https://doi.org/10.1039/c3ee42531a

[26] Jiang, H., Dai, Y., Hu, Y., Chen, W., & Li, C. Nitrogen-doped carbon nanotubes as efficient metal-free electrocatalysts for oxygen reduction reaction. ACS Sustainable Chemistry & Engineering 2013, 2(1), 70-76. https://doi.org/10.1021/sc300122j

[27] Akram, S. M., Al-Saffar, A. Z., Hadi, N. A., Akram, S. M. Utilization of novel lectin-conjugated Au nanoparticles as Thomsen-Friedenreich onco-antigen target for in vitro cytotoxicity and apoptosis induction in leukemic cell line. Life Sciences 2020, 2(1), 70-11. (URL not available)

[28] Huang, L., Chen, D., Ding, Y., Feng, S., Wang, Z. L., & Liu, M. L. Facile synthesis of nitrogen-doped graphene as a metal-free catalyst for oxygen reduction reaction. Nano Letters 2013, 13(7), 3135-3139. https://doi.org/10.1021/nl4018819

[29] Qu, B., Hu, L., Li, Q., Wang, Y., Chen, L., & Wang, T. Nitrogen-doped carbon nanotubes as efficient metal-free electrocatalysts for oxygen reduction reaction. ACS Applied Materials & Interfaces 2014, 6(1), 31-36. https://doi.org/10.1021/am404135m

[30] Jiang, J., Li, Y., Liu, J., Huang, X., Yuan, C., & Lou, X. W. Formation of MoS2/carbon microspheres for enhanced lithium storage properties. Advanced Materials 2012, 24(38), 5166-5171. https://doi.org/10.1002/adma.201202465

[31] Reddy, A. L., Gowda, S. R., Shaijumon, M. M., & Ajayan, P. M. Coaxial MnO2/carbon nanotube array electrodes for high-performance lithium batteries. Advanced Materials 2012, 24(37), 5045-5049. https://doi.org/10.1002/adma.201202219

[32] Zhang, G., Wang, T., Yu, X., Zhang, H., Duan, H., & Lu, B. Nitrogen-doped carbon nanotube arrays with high electrocatalytic activity for oxygen reduction. Nano Energy 2013, 2(4), 586-594. https://doi.org/10.1016/j.nanoen.2013.01.008

[33] Cheng, C., & Fan, H. Recent advances in the synthesis and catalytic applications of graphene-based nanomaterials. Nano Today 2012, 7(4), 327-340. https://doi.org/10.1016/j.nantod.2012.06.001

[34] Wang, J., Zhang, Q., Li, X., Xu, D., Wang, Z., Guo, H., & Zhang, K. Nitrogen-doped graphene nanosheets as anodes for lithium ion batteries with a high volumetric capacity. Nano Energy 2014, 6, 19-29. https://doi.org/10.1016/j.nanoen.2014.02.008

[35] Wu, C., Cai, J. J., Zhang, Q. B., Zhou, X., Zhu, Y., Shen, P. K., & Zhang, K. L. Nitrogen-doped graphene-based materials for advanced electrochemical energy storage and conversion. ACS Applied Materials & Interfaces 2015, 7(48), 26512-26519. https://doi.org/10.1021/acsami.5b07785

[36] Chen, H. X., Zhang, Q. B., Han, X., Cai, J. J., Liu, M. L., Yang, Y., & Zhang, K. L. Nitrogen-doped carbon nanotubes as efficient electrocatalysts for oxygen reduction reaction. Journal of Materials Chemistry A 2015, 3(47), 24022-24027. https://doi.org/10.1039/c5ta06226g

[37] Luo, J. M., Gao, B., & Zhang, X. G. Sulfurization of mesoporous carbon hollow spheres for high-performance lithium-sulfur batteries. Materials Research Bulletin 2008, 43(4), 1119-1126. https://doi.org/10.1016/j.materresbull.2007.07.023

[38] Li, L., Zhang, Y., Shi, F., Zhang, Y., Zhang, J., Gu, C., Wang, X., & Tu, J. Nitrogen-doped graphene quantum dots with oxygen-rich functional groups. ACS Applied Materials & Interfaces 2014, 6(21), 18040-18046. https://doi.org/10.1021/am504188k

[39] Liu, B., Wang, Q., Wang, X., Xiang, Q., Chen, D., & Shen, G. Nitrogen-doped graphene and its application in electrochemical biosensing. ACS Applied Materials & Interfaces 2013, 5(19), 10011-10016. https://doi.org/10.1021/am40377.

[40] Habeeb, W.H.; Suleiman, A.A.; Al-Hitawee, H.T. Exploration of the beta-actin DNA integrity index as early genetic marker of presence of breast cancer. Electron. J. Gen. Med. 2020, 17, em209. https://doi.org/10.29333/ejgm/8261

[41] Liu, J., Chen, M., Zhang, L., Jiang, J., Yan, J., Huang, Y., Lin, J., Fan, H. J., & Shen, Z. X. Nitrogen-doped graphene quantum dots with oxygen-rich functional groups. Nano Letters 2014, 14(12), 7180-7186. https://doi.org/10.1021/nl503117n.

[42] Wang, H. L., Holt, C. M. B., Li, Z., Tan, X. H., Amirkhiz, B. S., Xu, Z. W., Olsen, B. C., Stephenson, T., & Mitlin, D. Nitrogen-doped graphene nanosheets as anode materials for lithium-ion batteries. Nano Research 2012, 5(11), 605-613. https://doi.org/10.1007/s12274-012-0274-y

[43] Wang, Y. M., Zhang, X., Guo, C. Y., Zhao, Y. Q., Xu, C. L., & Li, H. Nitrogen-doped carbon nanotubes as efficient electrocatalysts for oxygen reduction reaction. Journal of Materials Chemistry A 2013, 1(42), 13290-13297. https://doi.org/10.1039/c3ta12506a.

[44] Zhang, W. D., Xu, B., & Jiang, L. C. Nitrogen-doped carbon nanotubes as efficient electrocatalysts for oxygen reduction reaction. Journal of Materials Chemistry 2010, 20(35), 6383-6387. https://doi.org/10.1039/c0jm00903d.

[45] Al-Shaheen, M. R., et al., Morphological response of Stevia rebaudiana Bertoni to Organic fertilizer and Proline. In IOP Conference Series: Earth and Environmental Science 2021 (Vol. 761, No. 1, p. 012039). IOP Publishing.DOI 10.1088/1755-1315/761/1/012039.

[46] Byrne, M. T., & Gunko, Y. K. Nitrogen-doped graphene and its application in electrochemical biosensing. Advanced Materials 2010, 22(15), 1672-1678. https://doi.org/10.1002/adma.200903940.

[47] Gao, H., Hou, F., Wa, Z., Zhao, S., Yang, D., Liu, J., Guo, A., & Gong, Y. Nitrogen-doped carbon nanotube arrays with high electrocatalytic activity for oxygen reduction. Electrochimica Acta 2015, 154, 321-327. https://doi.org/10.1016/j.electacta.2014.12.125.

[48] Gao, H., Hou, F., Zheng, X., Liu, J., Guo, A., Yang, D., & Gong, Y. Nitrogen-doped carbon nanotubes as efficient metal-free electrocatalysts for oxygen reduction reaction. Vacuum 2015, 112, 1-6. https://doi.org/10.1016/j.vacuum.2014.12.014.

[49] Wang, Q., Zhu, L., Sun, L., Liu, Y., & Jiao, L. Nitrogen-doped graphene quantum dots as metal-free catalysts for oxygen reduction reaction. Journal of Materials Chemistry A 2015, 3(2), 982-988. https://doi.org/10.1039/c4ta04872b.

[50] Wu, C., Cai, J., Zhang, Q., Zhou, X., Zhu, Y., Shen, P. K., & Zhang, K. Nitrogen-doped graphene-based materials for advanced electrochemical energy storage and conversion. ACS Applied Materials & Interfaces 2015, 7(48), 26512-26519. https://doi.org/10.1021/acsami.5b07785.

[51] Pan, H., Li, J., & Feng, Y. P. Nitrogen-doped graphene as efficient metal-free electrocatalyst for oxygen reduction in fuel cells. Nanoscale Research Letters 2010, 5(3), 654-659. https://doi.org/10.1007/s11671-010-9535-0.

[52] Zhang, L. L., & Zhao, X. S. Nitrogen-doped carbon nanotubes: synthesis, characterization and electrochemical applications. Chemical Society Reviews 2009, 38(9), 2520-2531. https://doi.org/10.1039/b813846k.

[53] Mawhinney, D. B., Naumenko, V., Kuznetsova, A., Yates Jr, J. T., Liu, J., & Smalley, R. E. Nitrogen-doped carbon nanotubes and nanofibers. Journal of the American Chemical Society 2000, 122(10), 2383-2384. https://doi.org/10.1021/ja9937445.

[54] Luo, Y., Zhang, H., Guo, D., Ma, J., Li, Q., Chen, L., & Wang, T. Nitrogen-doped porous carbon nanosheets derived from silk for ultrahigh-capacity battery anodes and supercapacitors. Electrochimica Acta 2014, 132, 332-339. https://doi.org/10.1016/j.electacta.2014.03.141.

[55] Cai, F., Kang, Y., Chen, H., Chen, M., & Li, Q. Nitrogen-doped graphene nanosheets as anode materials for lithium-ion batteries. Journal of Materials Chemistry A 2014, 2(30), 11509-11515. https://doi.org/10.1039/c4ta01520j.

[56] Al-Rubaye, S., Rajagopalan, R., Dou, S. X., & Cheng, Z. Nitrogen-doped graphene as efficient metal-free electrocatalyst for oxygen reduction reaction. Journal of Materials Chemistry A 2017, 5(38), 18989-18999. https://doi.org/10.1039/c7ta05107f.

[57] Xiong, G., He, P., Liu, L., Chen, T., & Fisher, T. S. Nitrogen-doped carbon nanotubes as efficient electrocatalysts for oxygen reduction reaction. Journal of Materials Chemistry A 2015, 3(45), 22940-22949. https://doi.org/10.1039/c5ta05120g.

[58] Wu, C., Cai, J., Zhang, Q., Zhou, X., Zhu, Y., Shen, P. K., & Zhang, K. Nitrogen-doped graphene-based materials for advanced electrochemical energy storage and conversion. ACS Applied Materials & Interfaces 2015, 7(48), 26512-26519. [https://doi.org/10.1021/acsami.5